

# Intensity Coding in Two-Dimensional Excitable Neural Networks

Mauro Copelli

Laboratório de Física Teórica e Computacional  
Departamento de Física, Universidade Federal de Pernambuco  
50670-901, Recife, PE, Brazil

Osame Kinouchi

Laboratório de Sistemas Neurais  
Departamento de Física e Matemática,  
Faculdade de Filosofia, Ciências e Letras de Ribeirão Preto  
Universidade de São Paulo, 14040-901, Ribeirão Preto, SP, Brazil

October 26, 2018

## Abstract

In the light of recent experimental findings that gap junctions are essential for low level intensity detection in the sensory periphery, the Greenberg-Hastings cellular automaton is employed to model the response of a two-dimensional sensory network to external stimuli. We show that excitable elements (sensory neurons) that have a small dynamical range are shown to give rise to a collective large dynamical range. Therefore the network transfer (gain) function (which is Hill or Stevens law-like) is an emergent property generated from a pool of small dynamical range cells, providing a basis for a “neural psychophysics”. The growth of the dynamical range with the system size is approximately logarithmic, suggesting a functional role for electrical coupling. For a fixed number of neurons, the dynamical range displays a maximum as a function of the refractory period, which suggests experimental tests for the model. A biological application to ephaptic interactions in olfactory nerve fascicles is proposed.

# 1 Introduction

Experimental results show that individual receptor neurons have a small dynamical range [1, 2]. Given a properly defined stimulus intensity  $r$  (e.g. light intensity for rods in the retina, or odorant concentration for sensory neurons in the olfactory epithelium), the response  $f(r)$  of a single neuron (e.g. the spike frequency) saturates at a value  $f_{max}$  for sufficiently large values of  $r$ . Defining  $r_{10}$  and  $r_{90}$  as the stimulus values for which the response attain 10% and 90% of  $f_{max}$ , the dynamical range  $\Delta r$  is usually defined [1] as

$$\Delta r = \log_{10} \left( \frac{r_{90}}{r_{10}} \right), \quad (1)$$

in log units. In other words, the dynamical range roughly measures the number of decades over which the stimulus can be properly discriminated<sup>1</sup>, discarding stimuli too faint to be considered “detected” ( $r < r_{10}$ ) or too close to saturation ( $r > r_{90}$ ). In olfactory receptor cells of the tiger salamander [1] and the frog [2],  $\Delta r \sim 1$  log unit (10 dB).

The psychophysics literature, on the other hand, shows that our ability to discriminate external signals of different kinds covers a *large* dynamical range [3]. This is reflected in phenomenological psychophysical laws used to fit data, which state that the psychological perception of a given stimulus  $r$  increases as  $\sim r^\alpha$ ,  $\alpha < 1$  (Stevens’ law), as  $\sim \log(r)$  (Weber-Fechner law), or as  $\sim r^\alpha / (c^\alpha + r^\alpha)$  (Hill function, which may be thought of as a saturating Stevens’ law). That is, differently from individual sensory neurons, organisms perform *signal compression*, being able to process environmental stimuli whose intensities usually span several orders of magnitude.

How can we reconcile these results? How could this signal compression be physically implemented considering that, at the very first stage of the signal processing, individual sensory neurons have a small dynamical range?

Following a conjecture put forward by Stevens [3], we propose that this signal compression occurs already at the periphery of the nervous system, that is, at the first “relevant” synaptic level. In our model,

---

<sup>1</sup>An alternative definition employs 5% and 95% of the saturation value for evaluating  $\Delta r$ . This is of course just a matter of choice. Our results remain qualitatively the same in either case.

this processing comes out naturally as a result of the collective phenomenon of *non-linear amplification* in excitable networks. While *individual* sensory neurons have a small dynamical range, an *array* of connected neurons can collectively exhibit a very large dynamical range.

The motivation for the model comes from recent experimental findings showing that electrical synapses by gap junctions are present in the periphery of different sensory systems, such as the olfactory glomeruli [4, 5] and the retina [6]. With this information at hand, we model a given sensory periphery as a two-dimensional array of excitable elements which are laterally connected by electrical synapses. Experimentally, the topology of the neural network connected by gap junctions is still not known, and specific details probably depend on the particular sensory system under consideration. So the two-dimensional lattice can be considered as the natural first step towards a biologically acceptable model. As a possible biological application, it could represent the cross section of a nerve fascicle containing highly packed unmyelinated axons coupled by electric interactions, which target a common secondary neuron, as found in the olfactory periphery. The one-dimensional case, which may be thought of as an approximation for networks where neurons are coupled to two neighbors in average, has been previously addressed in Ref. [7].

In section 2 we introduce the cellular automaton model used for each excitable element and briefly review results from the literature. Our results are discussed in section 3, while section 4 brings our concluding remarks and suggestions for experimental tests.

## 2 The model

In order to simulate large networks, we make use of the simplest possible model for an excitable element: an  $n$ -state cellular automaton (CA). The state of the  $i$ -th cell ( $i = 1, \dots, N$ ) at discrete time  $t$  is denoted by  $x_i(t) \in \{0, 1, \dots, n-1\}$ . A field  $h_i(t) \in \{0, 1\}$  indicates whether the stimulus at site  $i$  is supra- or sub-threshold. The CA model contains two ingredients:

1. a cell spikes in the next time step ( $x_i(t+1) = 1$ ) only if it is currently stimulated ( $h_i(t) = 1$ ) AND in its resting state ( $x_i(t) = 0$ )
2. after a spike, a refractory period takes place ( $x_i = 2, 3, \dots, n-1$ ),

during which no further spikes occur, until the cell returns to its resting state (formally, if  $x_i(t) > 0$ , then  $x_i(t+1) = [x_i(t) + 1] \bmod n$  with probability one)

This corresponds to one of the several variants of the model proposed by Greenberg and Hastings [8]. It was initially designed to provide a simple explanation for the mechanisms underlying pattern formation in excitable media. Indeed, the onset of self-sustained or re-entrant activity (with e.g. spiral waves) in a plethora of systems (including from heart tissue to chemical reactions) has been a research topic of considerable interest (see e.g. Refs. [9, 10] and references therein). Different flavors of the Greenberg-Hastings cellular automaton (GHCA) have been used in a variety of applications: collective oscillations of pyramidal cells in the hippocampus [11, 12]; noise-induced memory [13] and the evolution of the HIV infection [14]. In this paper we address an apparently unaccounted feature of the widely studied GHCA: the collective enhancement of the dynamical range of the single cells.

We model the response of a sensory neural network to some external input, and assume that this response vanishes if input is removed. This is accomplished with the rules defined above which, together with a resting initial condition ( $x_i(t=0) = 0, \forall i$ ) and the synchronous update of the lattice, prevent self-sustained activity from occurring [12]. We also assume that the input signal  $I_i(t)$  (which may have been pre-processed by earlier layers in a biological network) arriving on cell  $i$  at time  $t$  is a Poisson process of supra-threshold events of stereotyped unit amplitude. That is,  $I_i(t) = \sum_n \delta(t, t_n^{(i)})$  where  $\delta(a, b)$  is the Kronecker delta and the time intervals  $t_{n+1}^{(i)} - t_n^{(i)}$  are distributed exponentially with average (input rate)  $r$ , measured in events per second. At each time step, the probability of arrival (per neuron) of an external input is therefore

$$\lambda(r) = 1 - e^{-r\tau} , \quad (2)$$

where  $\tau = 1$  ms coincides with the approximate duration of a spike and is the time scale adopted for a time step of the model. With this choice, the number of states  $n$  of the GHCA corresponds roughly to the refractory period (measured in ms) of the sensory neurons (or the sensory axons).

The network connectivity is implicitly defined by the field  $h_i$ . For uncoupled cells, we have simply  $h_i^{(u)}(t) = I_i(t)$ , i.e. cells are excited

only by external stimuli. We model the coupling via gap junctions with the field

$$h_i^{(c)}(t) = 1 - [1 - I_i(t)] \prod_j [1 - \delta(x_j(t), 1)] , \quad (3)$$

i.e. cells are excited by external stimuli or at least one spiking cell  $j$  (where  $j$  runs over the neighborhood of  $i$ ). We have employed periodic as well as open boundary conditions, with indistinguishable results. The number of sites in the regular lattice with coordination number  $z$  is  $N = N_x N_y$ .

The response  $F(r)$  of the lattice to a given stimulus intensity  $r$  is given by the mean firing rate per cell in a long time interval  $T$  (typically we have used  $T = \mathcal{O}(10^5)$  time steps). This should be compared to the mean firing rate per cell  $f$  of an ensemble of uncoupled cells, whose dependence on  $r$  can be exactly calculated:

$$f(r) = \frac{\lambda(r)}{1 + (n-1)\lambda(r)} . \quad (4)$$

This linear saturating function will be the benchmark against which results from the lattices should be compared. Note that, with the definition of Eq. 1, uncoupled cells have a dynamical range

$$\Delta r = \log_{10} \left\{ \frac{\ln \left[ 1 + \frac{9}{n} \right]}{\ln \left[ 1 + \frac{1}{9n} \right]} \right\} , \quad (5)$$

which is a smooth curve and, for moderate values of  $n$ , is well approximated by the asymptotic value  $\Delta r \stackrel{n \rightarrow \infty}{\simeq} \log_{10}(81) \simeq 19$  dB. This dynamical range is slightly larger than the experimental results, but still too small to account for psychophysical data [3].

### 3 Results and Discussion

For very low values of  $r$ , the stimulation of a single site generates a wave of activation which propagates through the entire lattice (see Fig. 1(a)). Before another stimulus is produced, the wave front is annihilated at the walls (with open boundary conditions) or when it touches itself (with periodic boundary conditions), because sites which have spiked in the last  $n-1$  time steps cannot spike again due to the

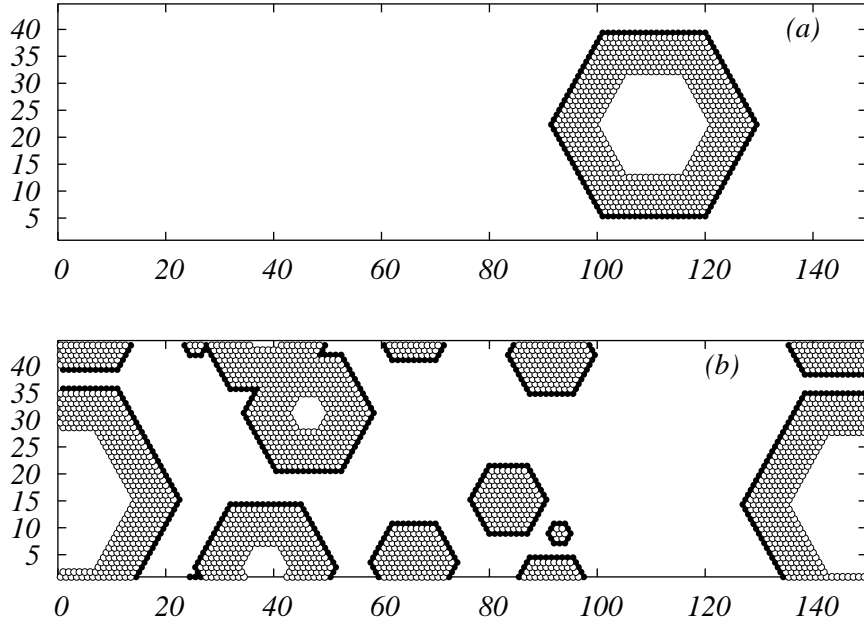


Figure 1: Snapshots of a triangular  $150 \times 50$  lattice where 10-state CA interact with their  $z = 6$  nearest neighbors (periodic boundary conditions). Closed circles:  $x_i(t) = 1$  (spiking). Open circles:  $2 < x_i(t) < n$  (refractory). Background:  $x_i(t) = 0$  (resting). Panel (a):  $r = 0.005 \text{ s}^{-1}$ . Panel (b):  $r = 0.1 \text{ s}^{-1}$ .

refractory period. In this regime, a single stimulus produces  $N$  spikes, yielding an  $N$ -fold amplification,

$$F \stackrel{r \simeq 0}{\simeq} N\lambda \simeq Nr\tau . \quad (6)$$

At the other extreme, for very high values of  $r$  the propagation of waves is suppressed by excess of external stimulus: in this regime, the coupling becomes irrelevant since each cell is already spiking at its maximal rate,

$$F \stackrel{r \rightarrow \infty}{\simeq} f \simeq \frac{1}{n} \equiv F_{max} , \quad (7)$$

yielding no amplification,  $F/f \simeq 1$ .

In between those two regimes, waves are created, propagate and annihilate when meeting one another, yielding complex geometric patterns which appear from the remains of partially destroyed waves (see

Fig. 1(b)). The interplay between wave creation and wave annihilation provides the self-limited mechanism by which the amplification  $F/f$  decreases smoothly from  $\mathcal{O}(N)$  (for small  $r$ ) to  $\mathcal{O}(1)$  (for large  $r$ ). This is a mechanism which leads to signal compression.

Fig. 2(a) shows the result of numerical simulations for square lattices with  $z = 8$  and  $n = 10$  in a log-log plot. The linear response (Eq. 6) for low values of  $r$  can be clearly seen at the leftmost portion of the graph, requiring lower values of  $r$  for larger system sizes (for a fixed low value of  $r$ , the larger the system the more probable it is for two excitable waves to interact). As  $r$  increases, wave annihilation starts competing with wave creation, bending down the nonlinear response. Finally, saturation ensues for values of  $r$  close to  $1/n$ , making the coupled and uncoupled cases nearly indistinguishable. The enhancement of the dynamical range becomes clear when we plot  $F(r)$  in a linear-log plot [Fig. 2(b)]: since the amplification due to coupling is larger for lower  $r$ , the curves stretch upward, compressing more decibels of stimuli in the same  $[0.1F_{max}, 0.9F_{max}]$  response interval.

The dimensionality of the lattice has a significant impact on the collective response, as exemplified by the results for a one-dimensional chain in Fig. 2. The differences can be understood as consequences of the following factors: a) in 1D wave fronts have a constant size (2 sites), while in 2D their size grows with time; b) because of a), waves in 2D can be partially destroyed (as exemplified in Fig. 1), while in 1D they are completely annihilated upon collision; c) the time it takes for a wave to reach the borders scales with  $N$  in 1D, but with  $\sqrt{N}$  in 2D. The combination of factors (a), (b) and (c) gives rise to finite size effects which are much stronger in 2D than in 1D. As Fig. 2 shows, for example, 1D chains with 1600 or 400 neurons would have essentially the same dynamical range, since finite size effects appear below  $r_{10} = 10$  Hz. For 2D lattices, on the other hand, the dynamical range changes.

We have simulated two-dimensional square lattices with  $z = 4$  and  $z = 8$  neighbors, as well as triangular lattices with  $z = 6$ . For a fixed dimensionality, the differences in coordination number are not important to our investigations, as can be seen in Fig. 2 (the curve for  $z = 6$  falls between those of  $z = 4$  and  $z = 8$ ). In what follows, we focus on results for  $z = 8$ .

For a given refractory period  $n$ , the size of the lattice regulates the crossover from the linear to the nonlinear response. If the sensitivity level  $r_{10}$  lies within the linear regime (as it does, for instance, in Fig. 2),

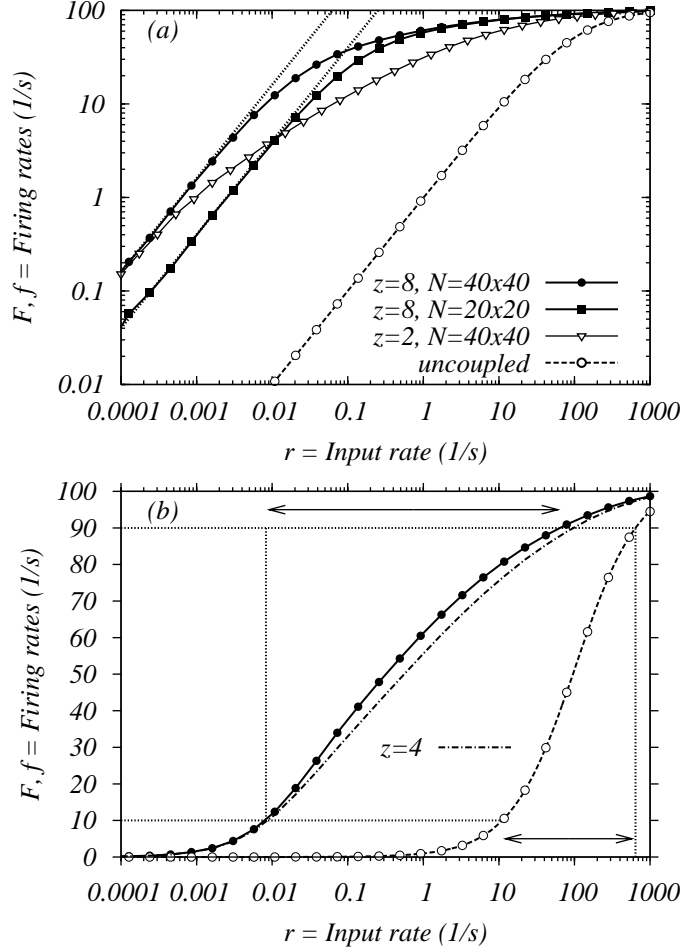


Figure 2: Response curves for square lattices of 10-state automata. (a) coupled ( $F$ , filled symbols) and uncoupled ( $f$ , open symbols) cases for  $z = 8$  neighbors. The dashed line corresponds to the exact solution (Eq. 4), while the dotted lines are the linear approximation, Eq. 6. Open triangles are results for a one-dimensional coupled system; (b) Linear-log version of (a), with the dot-dashed line representing a square lattice with  $N = 40 \times 40$  and  $z = 4$  neighbors. Arrows indicate the dynamical range.

then the dynamical range will be affected by the system size. It is important to note that this is not an artificial feature due to the somewhat arbitrary definition of  $\Delta r$ . Any reasonable definition of



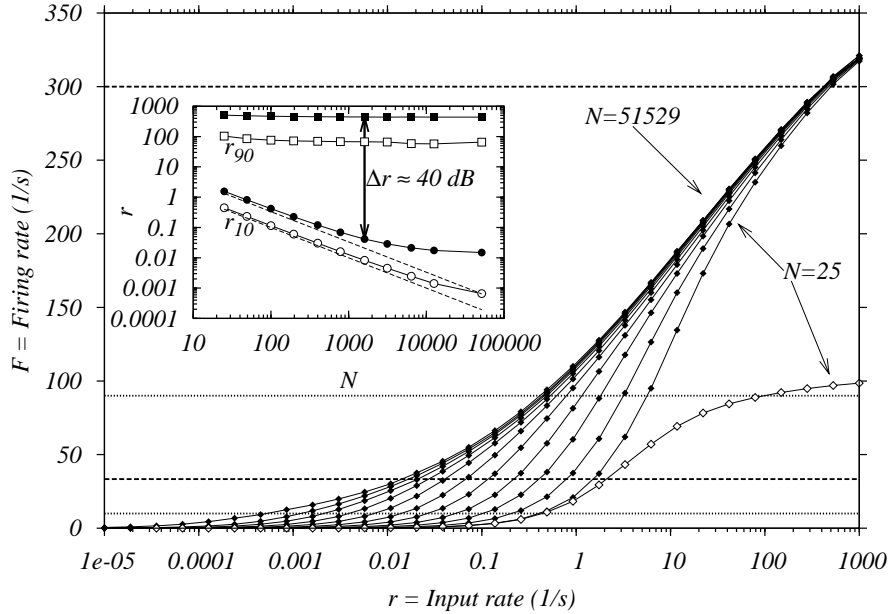


Figure 3: Response curves of 3–state (filled diamonds) and 10–state (open diamonds) automata for different lattice sizes  $N$  ( $N = 25$  for  $n = 3$  and 10, up to  $N = 51529$  for  $n = 3$ ). The upper (lower) horizontal line corresponds to 90% (10%) of the saturation firing rate for  $n = 3$  ( $F_{max} = 1/3 \text{ ms}^{-1} \simeq 333 \text{ s}^{-1}$ , thick dashed) and  $n = 10$  ( $F_{max} = 1/10 \text{ ms}^{-1} \simeq 100 \text{ s}^{-1}$ , thin dotted). Inset: sensitivity ( $r_{10}$ , circles) and saturation ( $r_{90}$ , squares) levels (filled symbols for  $n = 3$ , open symbols for  $n = 10$ ) as a function of the number of sites  $N$  in the lattice. The vertical arrow illustrates the dynamical range for a  $40 \times 40$  lattice with  $n = 3$ . Dashed lines correspond to Eq. 8.

the dynamical range will reveal a sensitivity gain (decrease in  $r_{10}$ ) for increasing values of  $N$ , as depicted in the family of curves of Fig. 3. Note that the saturation level  $r_{90}$  also changes, but much less than  $r_{10}$ , leading to an enhancement of the dynamical range.

It is also worth mentioning that, since  $r_{10}$  and  $r_{90}$  are defined only relative to a saturation response, these quantities will depend on  $n$ . Fig. 3 and its inset illustrate this fact for  $n = 3$  (filled symbols) and  $n = 10$  (open symbols). Note that the relative meaning of “sensitivity” and “saturation” explains the following apparent contradiction: even though the  $n = 3$  curves lie *above* the  $n = 10$  curves (for the same

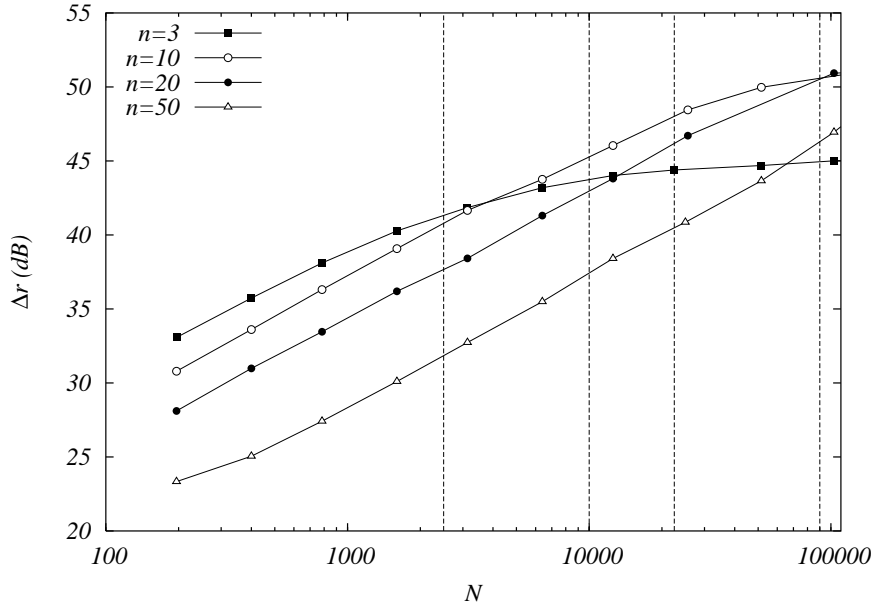


Figure 4: Dynamical range as a function of the lattice size for different values of  $n$ . The vertical lines indicate values of  $N$  to be considered in more detail subsequently.

system size), their sensitivity and saturation levels *also lie above* those of the  $n = 10$  case. In other words, if  $r_{10}$  is assumed to lie in the linear regime, then Eqs. 2 and 6 yield a decreasing dependence on  $N$  and  $n$ :

$$r_{10} \simeq -\frac{1}{\tau} \ln \left( 1 - \frac{0.1}{nN} \right). \quad (8)$$

This approximation is acceptable for moderate values of  $N$  (above which the interference among excitable waves invalidates the linearity assumption) and improves for increasing  $n$  (since this lowers  $r_{10}$  into the linear region — see inset of Fig. 3).

The above discussion only emphasizes that the dynamical range stands out as a better quantity to look at than  $r_{10}$  and  $r_{90}$ , being a bona fide *dimensionless* variable which could be compared to experimental data. The dependence of  $\Delta r$  on the system size can be seen in Fig. 4. Note that an expansion in Eq. 8 for  $N \gg 0.1/n$  yields

$$\Delta r(N) \simeq \log_{10}(r_{90}) + \log_{10}(10\tau nN). \quad (9)$$

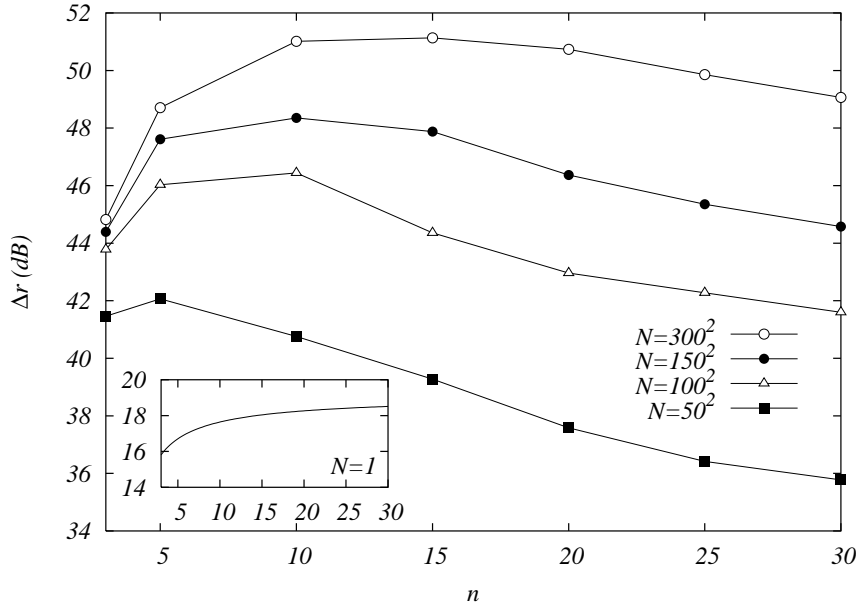


Figure 5: Dynamical range as a function of the refractory period  $n$  for different values of the lattice size. Inset: exact expression for an isolated neuron (Eq. 5).

If we neglect the (weak) dependence of  $r_{90}$  on  $N$ , this expression explains the approximately logarithmic growth in Fig. 4 before the curves level off. For larger values of  $N$ , the linearity assumption for  $r_{10}$  breaks down and Eqs. 8 and 9 are no longer valid.

In Fig. 4 one observes that for low values of  $N$  (say, up to  $\mathcal{O}(10^3)$ ), lower values of  $n$  imply larger dynamical ranges (this cannot be inferred from Eq. 9 since it omits the unknown and strong dependence of  $r_{90}$  on  $n$ ). As  $N$  grows, however, the curves in Fig. 4 start leveling off for increasing values of  $n$ . This simple fact has very interesting consequences. Suppose that we fix the system size at one of the four values specified by the vertical lines in Fig. 4. If we now vary the refractory period  $n$ , we obtain the four curves displayed in Fig. 5, which have a maximum.

If we accept the reasoning that a large dynamical range is a desirable property for a live organism, then the results presented so far suggest two biological outcomes: first, that it would be advantageous for the organism to have as many sensory cells as possible. By elec-

trically coupling them, an increase of more than 100% in dynamical range could be obtained, as compared to isolated neurons (see inset of Fig. 5). This is supported by the experimental evidence that gap junctions are present in the sensory periphery (which was in fact what motivated the model [7]). Recent experiments in the mammalian retina [6] show that knocking out the gene responsible for connexin-36 (which accounts for the neuron-neuron gap junction channels) leads to a dramatic decrease in the dynamical range of ganglion cell responses.

However, the number of receptor neurons in a given sensory subsystem is usually limited by several factors, from metabolic costs to sheer occupied space (for instance, each olfactory glomerulus of the rabbit receives input from  $\mathcal{O}(10^4)$  sensory neurons [15]). This leads to the second biological suggestion. Fig. 5 suggests that for a given fixed size of the subsystem, it would be advantageous for an organism to set the refractory period of the receptor neurons to the value  $n_{max}$  that yields the maximum dynamical range. Since  $n_{max}(N)$  seems to be an increasing function, we could expect the size of connected neuron patches and the refractory period of the neurons (which classically are two independent parameters) to be correlated. In other words, smaller patches would tend to have neurons with shorter refractory period. Naturally, it is important to check the robustness of these results in other models of excitable media before specific experimental tests could be proposed.

## 4 Concluding Remarks

We have presented results concerning the nonlinear response of the two-dimensional GHCA to a Poisson stimulus. In particular, the coupling between the excitable elements has been shown to greatly enhance the dynamical range due to the collective phenomenon of self-limited amplification of excitable waves.

We stress that we do not claim this is the *only* explanation for the enhancement of the dynamical range. Variation of the values of  $r_{10}$  and  $r_{90}$  within the population of receptor neurons, for instance, is another hypothesis. In that scenario, different stimulus ranges would “recruit” different groups of neurons, therefore leading to an overall enhancement of the dynamical range (even if the neurons were *uncoupled*). Theoretical work in this direction by Cleland and Linster [16] has shown that this could in principle be achieved by heterogeneous

overexpression of odorant receptors in the olfactory epithelium. Note, however, that doubling the dynamical range of the ensemble (as compared to that of individual neurons) would require the order of a hundred-fold overexpression of receptors, in that model. As Cleland and Linster point out, “measured spare receptor capacities in intracortical and culture systems studied to date are typically less than twofold” [16].

Interestingly, the different proposed mechanisms are not mutually exclusive. In fact, “recruitment” as described above could in principle coexist with the self-limited amplification we propose. And both could cooperate with further nonlinear post-processing of the signals (e.g. by mitral cell integration in the olfactory bulb). We believe that the strength of our model lies on two central issues. The first one is experimental evidence: the model suggests a functional role for the electrical synapses by gap junctions which have been experimentally found in the sensory periphery. The second point is that the mechanism is *simple*. Indeed, the model relies more generally on lateral excitation, and could in principle even forego gap junctions specifically. In the olfactory nerve, for instance, it could be implemented via the electrical coupling mediated by ephaptic interactions among neighboring axons, which have recently been modeled by Bokil et al. [17]. Neuronal circuits where mutual bidirectional excitation by chemical synapses occur could also be subjected to a similar modeling.

The general question of how brains represent sensory stimuli is a classical and very difficult one, and has been addressed by physicists like Fechner, Plateau and Maxwell. Our model addresses only part of the problem, containing a mechanism to enhance the coding of a very basic (perhaps the most basic) property of the senses: intensity of the stimulus.

Consider, for instance, the retina. Our primary concern is with electrical coupling not at networks of non-spiking neurons (as cones, horizontal cells etc) but at excitable networks of spiking cells. So we are interested in wave generation and synchronization at the first relevant spiking network (ganglion cell layer, in the case of vision) as a candidate mechanism for intensity coding in the output of optic nerve fibers. So, the “input” level  $r$  presented in our model should be interpreted as the input to the appropriate excitable network which we speculate to be situated at the ganglion level, not the raw input to the retina. There is experimental evidence that the spikes of ganglion cells are correlated with small latency (typical of electrical

coupling) [18, 19], which is consistent with our model. For specificity coding, on the other hand, other mechanisms seem best suited, such as lateral inhibition (which is well established in the literature, occurring in previous layers [20]). The olfactory epithelium, on the other hand, has no known topographical structure in the expression of different receptors, presenting “mosaic” receptor expression [21]. In this case, the excitable elements of the model could be thought of as unmyelinated axons inside an olfactory nerve fascicle (which are known to pertain to a single class of receptors and innervate a single glomerulus). Thus the model gives a potential explanation to the large dynamical range observed in the intensity coding of individual glomeruli, but not to the much more difficult problem of how the identity of different smells are combinatorially coded by the several glomeruli.

Real neurons are obviously much more complex than the our simple CA model: refractory periods are not necessarily absolute, responses can come in form of bursts, adaptive firing etc. However, we have also examined more biologically realistic models previously, leading to results similar to those of the GHCA [7, 22]. The robustness of the results presented in this contribution with respect to different excitable models, lattice connectivity and stimulus statistics is the subject of ongoing research. For instance, non-homogeneous two-dimensional lattices have been known to produce self-sustained activity (spiral waves) since the seminal work of Wiener and Rosenblueth [23]. It remains to be investigated *how* to connect excitable elements in order to maximize the dynamical range of the collective response, but also suppressing spiral waves.

Despite its lack of biological realism, the CA approach is extremely useful since it allows the simulation of large networks and even the calculation of collective properties under appropriate approximations. Indeed, analytical tools such as hierarchical mean field approximations [24] are available for studying cellular automata. We have obtained good results for the one-dimensional system with a mean field approximation at the pair level [25], which analytically reveals the low- $r$  signal compression. The single site mean field approximation for the GHCA fails in hypercubic lattices of any dimension, and we are currently investigating the next hierarchical step to analyze the two-dimensional system. It is interesting to point out, however, that unless the mean field calculation contains finite size corrections, it may not be the best tool for understanding the phenomena occurring in finite cell assemblies. As has been previously noticed regarding the

olfactory nerve fascicles, many interesting biological phenomena occur precisely at intermediate values of the lattice size, which emphasizes the usefulness of computer simulations in addition to analytical results that must assume large  $N$  (thermodynamic) limits.

**Acknowledgments** Invaluable discussions with R. F. Oliveira and A. C. Roque are gratefully acknowledged. The authors also thank the anonymous referees for interesting suggestions and comments. MC acknowledges support from Projeto Enxoval (UFPE), CNPq, FACEPE, CAPES, and special program PRONEX. OK acknowledges support from FAPESP and CNPq.

## References

- [1] S. Firestein, C. Picco, and A. Menini. The relation between stimulus and response in olfactory receptor cells of the tiger salamander. *Journal of Physiology*, 468:1–10, 1993.
- [2] J.-P. Rospars, P. Lánský, P. Duchamp-Viret, and A. Duchamp. Spiking frequency versus odorant concentration in olfactory receptor neurons. *BioSystems*, 58:133–141, 2000.
- [3] S. S. Stevens. *Psychophysics: Introduction to its Perceptual, Neural and Social Prospects*. Wiley, New York, 1975.
- [4] T. Kosaka and K. Kosaka. Neuronal gap junctions in the rat main olfactory bulb, with special reference to intraglomerular gap junctions. *Neuroscience Research*, 45:189–209, 2003.
- [5] C. Zhang and D. Restrepo. Heterogeneous expression of connexin 36 in the olfactory epithelium and glomerular layer of the olfactory bulb. *J. Comp. Neurol.*, 459:426–439, 2003.
- [6] M. R. Deans, B. Volgyi, D. A. Goodenough, S. A. Bloomfield, and D. L. Paul. Connexin36 is essential for transmission of rod-mediated visual signals in the mammalian retina. *Neuron*, 36:703–712, 2002.
- [7] M. Copelli, A. C. Roque, R. F. Oliveira, and O. Kinouchi. Physics of Psychophysics: Stevens and Weber-Fechner laws are transfer functions of excitable media. *Phys. Rev. E*, 65:060901(R), 2002.
- [8] J. M. Greenberg and S. P. Hastings. Spatial patterns for discrete models of diffusion in excitable media. *SIAM J. Appl. Math.*, 34:515–523, 1978.

- [9] D. T. Kaplan, J. M. Smith, B. E. H. Saxberg, and R. J. Cohen. Nonlinear dynamics in cardiac conduction. *Math. Biosci.*, 90:19–48, 1988.
- [10] A. Bardou, S. Achour, P. Auger, and J.-L. Chassé. Effects of local ischemia and transient conduction blocks on the induction of cardiac reentries. *Int. J. Bifurcat. Chaos*, 6:1657–1664, 1996.
- [11] R. D. Traub, D. Schmitz, J. G. R. Jefferys, and A. Draguhn. High-frequency population oscillations are predicted to occur in hippocampal pyramidal neuronal networks interconnected by axoaxonal gap junctions. *Neuroscience*, 92:407–426, 1999.
- [12] T. J. Lewis and J. Rinzel. Self-organized synchronous oscillations in a network of excitable cells coupled by gap junctions. *Network: Comput. Neural Syst.*, 11:299–320, 2000.
- [13] D. R. Chialvo, G. A. Cecchi, and M. O. Magnasco. Noise-induced memory in extended excitable systems. *Phys. Rev. E*, 61:5654–5657, 2000.
- [14] R. M. Zorzenon dos Santos and S. G. Coutinho. On the dynamics of the HIV infection. *Phys. Rev. Lett.*, 87:168102, 2001.
- [15] G. M. Shepherd, editor. *The Synaptic Organization of the Brain*. Oxford University Press, 1998.
- [16] T. A. Cleland and C. Linster. Concentration tuning mediated by spare receptor capacity in olfactory sensory neurons: A theoretical study. *Neural Computation*, 11:1673–1690, 1999.
- [17] H. Bokil, N. Laaris, K. Blinder, M. Ennis, and A. Keller. Ephaptic interactions in the mammalian olfactory system. *J. Neurosci.*, 21:RC173, 2001.
- [18] W. Bair. Spike timing in the mammalian visual system. *Curr. Opin. Neurobiol.*, 9:447–453, 1999.
- [19] S. Hidaka, T. Kato, and E. Miyachi. Expression of gap junction connexin36 in adult rat retinal ganglion cells. *J. Integr. Neurosci.*, 1(1):3–22, 2002.
- [20] D. Purves, G. J. Augustine, D. Fitzpatrick, W. C. Hall, A.-S. Lamantia, J. O. McNamara, and S. M. Williams. *Neuroscience*. Sinauer Associates, second edition, 2000.
- [21] F. M. Simões-de-Souza and A. C. Roque. A biophysical model of vertebrate olfactory epithelium and bulb exhibiting gap junc-



- tion dependent odor-evoked spatiotemporal patterns of activity. *Biosystems*, 73(1):25–43, 2004.
- [22] M. Copelli, R. F. Oliveira, A. C. Roque, and O. Kinouchi. Signal compression in the sensory periphery. *Neurocomputing*, 2005. To appear.
- [23] N. Wiener and A. Rosenblueth. The mathematical formulation of the problem of conduction of impulses in a network of connected excitable elements, specifically in cardiac muscles. *Arch. Inst. Cardiol. Mexico*, 16:205–265, 1946.
- [24] T. Tomé and M. J. Oliveira. *Dinâmica Estocástica e Irreversibilidade*. EDUSP, São Paulo, 2001.
- [25] L. S. Furtado and M. Copelli. In preparation.